UNCLASSIFIED

AD NUMBER

AD390306

CLASSIFICATION CHANGES

TO: **unclassified**

FROM: **confidential**

LIMITATION CHANGES

TO:

Approved for public release, distribution unlimited

FROM:

Distribution: DoD only: others to Director, Naval Research Lab., Washington, D. C. 20390.

AUTHORITY

NRL ltr, 17 Jul 2002; NRL ltr, 17 Jul 2002

THIS PAGE IS UNCLASSIFIED

CONFIDENTIAL

AD 390 306 L

CLASSIFICATION CHANGED
TO: CONFIDENTIAL
FROM: SECRET
AUTHORITY:
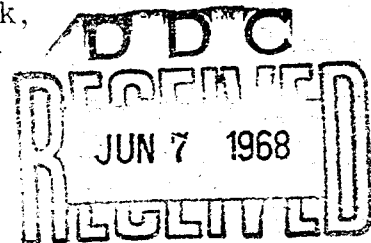— DOD 5200.1-R Nov 73

S.C

SECRET

MADRE PERFORMANCE

PART 4 - OBSERVATIONS OF FEBRUARY 15, 1962

[UNCLASSIFIED TITLE]

F. M. Gager, G. A. Morgan, W. C. Headrick,
C. B. Tesauro, and E. N. Zettle

Radar Techniques Branch
Radar Division

DDC
RECEIVED
JUN 7 1968
D

January 27, 1964

DDC CONTROL
NO. 62456

U. S. NAVAL RESEARCH LABORATORY
Washington. D.C.

SECRET

AD390306

PREVIOUS REPORTS IN THIS SERIES

NRL Report 5862, "Madre Performance, Part 1 – Observations of January 18 and 25, 1962" (Secret Report, Unclassified Title), F. M. Gager, W. C. Headrick, G. A. Morgan, F. H. Utley, and E. N. Zettle, Dec. 1962

NRL Report 5898, "Madre Performance, Part 2 – Observations of February 8, 1962" (Secret Report, Unclassified Title), F. M. Gager, W. C. Headrick, G. A. Morgan, D. C. Rholfs, C. B. Tesauro, and E. N. Zettle, Feb. 1963

NRL Report 5991, "Madre Performance, Part 3 – Observations of February 12, 1962" (Secret Report, Unclassified Title), F. M. Gager, G. A. Morgan, Christine B. Tesauro, G. A. Skaggs, and E. N. Zettle, Aug. 1963   AD- 344 106

SECURITY

(14) NRL ▮▮▮▮ 6019

(6) MADRE PERFORMANCE.

PART 4 - OBSERVATIONS OF FEBRUARY 15, 1962.

[UNCLASSIFIED TITLE]

(7) [VERY LONG RANGE, OVER-THE-HORIZON DETECTION OF AIRCRAFT WITH THE MADRE RADAR.

PART 4 - OBSERVATIONS OF FEBRUARY 15, 1962 (S).

[SECRET TITLE]

(9) Interim rept.,

F. M. Gager, G. A. Morgan, W. C. Headrick, C. B. Tesauro, and E. N. Zettle

Radar Techniques Branch
Radar Division

(11) January 27, 1964

U. S. NAVAL RESEARCH LABORATORY
Washington. D.C.

DDC CONTROL
NO. 56

ABSTRACT
[Secret]

The Madre radar was operated on February 15, 1962, to observe a USAF KC-135 aircraft over the North Atlantic Ocean at ranges of 500 to about 900 nautical miles. HF propagation conditions were unusual during the critical portions of the flight, and four ionospheric reflection layers were supported, a situation which provided data for multipath analysis. The analysis shows that in conditions of multipath propagation it is possible to resolve the paths and to obtain good over-the-ground ranges to targets and good true radial speed. Multipath conditions result in recording errors smaller than the range equivalent of the pulse length.

PROBLEM STATUS

This is an interim report on one phase of the problem; work is continuing on this and other phases.

AUTHORIZATION

NRL Problem R02-23
Project RF 001-02-41-4007
AF MIPR (30-602) 63-2928
(30-602) 63-2929
(30-602) 63-2995

VERY LONG RANGE, OVER-THE-HORIZON DETECTION
OF AIRCRAFT WITH THE MADRE RADAR
PART 4 – OBSERVATIONS OF FEBRUARY 15, 1962
[Secret Title]

INTRODUCTION

In addition to the use of naval aircraft, NRL has obtained flight support through the cooperation of the Rome Air Development Center for the evaluation of the Madre system. KC-135 jet tankers were flown on round trips from Griffiss Air Force Base, with the flight path chosen to be radial from about 600 naut mi to 1600 naut mi from the Madre site. The KC-135 aircraft were equipped with NRL beacon transponders, which were used to positively identify the aircraft.

Missions were flown by the Air Force on December 7, 9, and 21, 1961, and on February 9 and 15, 1962. Other successful missions have been flown since February 15; however, this report covers only the five flights through February 15; and of these five, the February 15 flight was the only one successfully tracked. Failure to obtain information on four of the flights was due to priority use of the available Madre operating frequencies by naval communications, faulty hf communication with the aircraft, radar system difficulties, and lack of a suitable propagation path at the available frequencies during critical portions of the flights.

KC-135 FLIGHT, FEBRUARY 15, 1962

The Bureau of Standards' propagation conditions for this date were "poor to fair" between 6 a.m. and 12 noon and "fair to good" 12 noon to 6 p.m. EST for this area. This flight was identified via the beacon transponders from 1450 to about 500 naut mi. However, skin detection of the KC-135 was verifiable only on the return flight from 900 naut mi to about 500 naut mi because of interference on the beacon frequencies and rather abnormal ionospheric conditions. Ionospheric conditions supported four reflection layers. They were E sporadic at 101 km, critical frequency 3.8 Mc; E at 115 km, critical frequency 2.95 Mc; and F_1 at 200 km merging with F_2 at 290 km with F_2 critical at 7 Mc. These propagation conditions provided an opportunity to examine performance under severe multipath conditions and demonstrated that the range error between paths is not serious.

The backscatter pattern at 1510 EST for the operating frequency 13.68 Mc is shown in Fig. 1. At this time the first hop backscatter range was 560 to 1200 naut mi and was actually made up of refraction by the E_s, E, and F layers of the ionosphere. The time vs calculated range of the KC-135 aircraft as determined from Air Force supplied position data is shown in Fig. 2.

Multipath conditions are such that if one assumes two one-way paths available, three slant ranges are possible to a given point. Thus energy can (a) go out and return via path one, (b) go out and return via path two, and (c) go out via path one and return via path two or vice versa. With four one-way paths available, E_s, E, F_1, and F_2, one can get up to ten possible slant ranges, differing by a small percentage error, for a given ground range. The ten paths are F_2, $F_2 + F_1$, $F_2 + E$, $F_2 + E_s$, F_1, $F_1 + E$, $F_1 + E_s$, E, $E + E_s$, and E_s. All paths are equally probable with an idealized ionosphere. It is believed that all of these appear in the data presented at least once except $F_2 + E_s$.
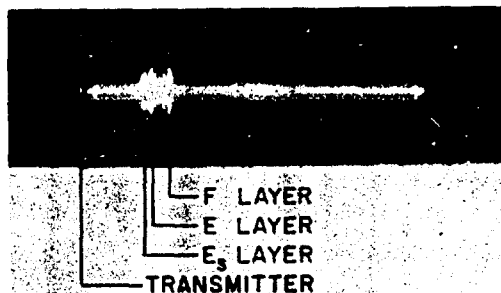
Fig. 1 - Backscatter intensity vs
range for 13.68 Mc at 1510 EST
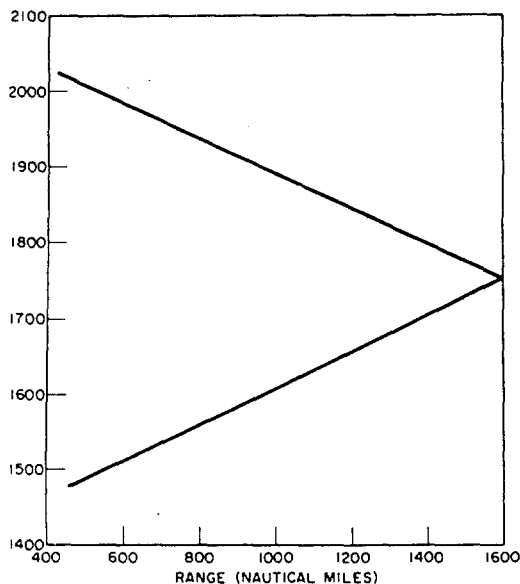on February 15, 1962

RANGE (NAUTICAL MILES)

Fig. 2 - Time vs great circle ground
range of the KC-135 aircraft during
the round trip as calculated from the
navigator's position data

In order to determine which paths were present a simplified view of the ionosphere
was taken, in which each layer was assumed to be a thin reflecting shell. It is realized
that this is an oversimplified picture and that the rays do not actually travel the paths
described. But the calculations which can readily be made permit significant comparisons
between signals to afford reasonable explanation of the seemingly erratic scattering of
points in a track acquired under multipath conditions.

In these calculations, the earth was assumed to be a perfect sphere of radius 3433.0
naut mi, a value chosen to minimize the spherical-assumption error for the region of
interest. The heights above the earth's surface of the assumed concentric reflecting
spherical shells corresponded to the Bureau of Standards virtual layer heights at the time,
as determined by vertical incidence sounding at Washington, D.C. Transparency of the
lower layers was assumed.

If one neglects the aircraft and transmitter heights above the surface of the earth,
the ray diagrams are as shown in Fig. 3. By the laws of reflection, $\phi_1 = \phi_2$, and since
$\overline{OT} = \overline{OA}$, triangles TOP and AOP are congruent. Therefore, $\theta_1 = \theta_2 = 1/2$ ground dis-
tance and $\ell_1 = \ell_2 = 1/2$ slant range.

The solution is obvious but is in rather severe error because of the actual heights of
aircraft and transmitter above the earth. Figure 4a shows the effect of considering these

heights. The downgoing portion of each ray has been foreshortened by the length of the "shadow" of the aircraft, and symmetry has been disturbed. The foldover diagram in Fig. 4b shows the relationship between corresponding components of the triangles in this condition. In this figure R_a is the radius of the aircraft path (R_0 plus the flight altitude), R_t is R_0 plus the antenna height, R_i is R_0 plus the layer height, a_t is the vertical angle of departure of the ray at the antenna, and a_a is the vertical angle of arrival of the ray at the aircraft.

A = AIRCRAFT
T = TRANSMITTER
O = CENTER OF EARTH
R_0 = EARTH RADIUS
SUBSCRIPTS IDENTIFY LAYERS
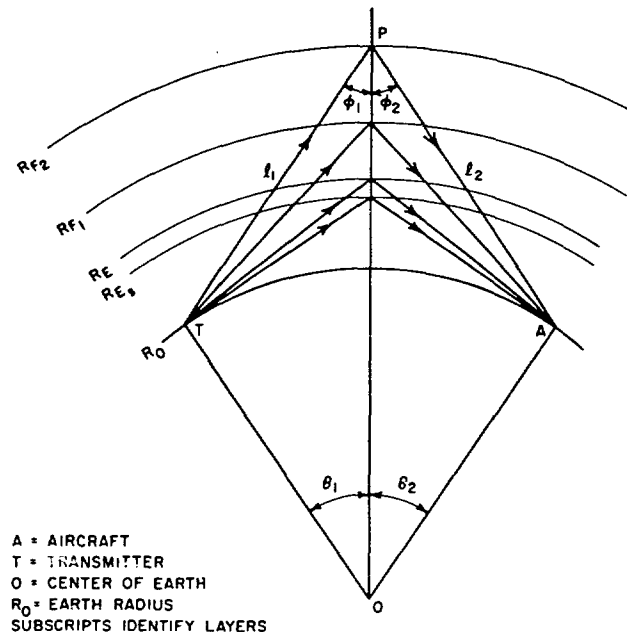
Fig. 3 - Ray diagram for reflection at the
various ionospheric layers

For this problem, with a known ground distance ($\theta_1 + \theta_2$) one could by successive approximation find the slant range for any assumed height. By doing this for each of the four layers in turn at each ground distance one could sort the signals into the probable responsible layers. Alternatively one could take each slant range ($\ell_1 + \ell_2$) and find the ground range for each layer height in turn, and in comparison with the navigational ground range identify the probable layer. Where many signals are to be sorted, a more straightforward and equally valid method is to trace out a range separation vs slant range profile for each layer by assigning values to a_t and solving for ℓ and θ. The profiles of the paths involving two layers can then readily be determined from the four single layer profiles, since the range separation for the combination path is the mean of the individual layer separations.

By use of this last method we obtained ten separation vs range profiles corresponding to the ten possible paths and then matched the data as closely as possible to select the most probable path for each signal.
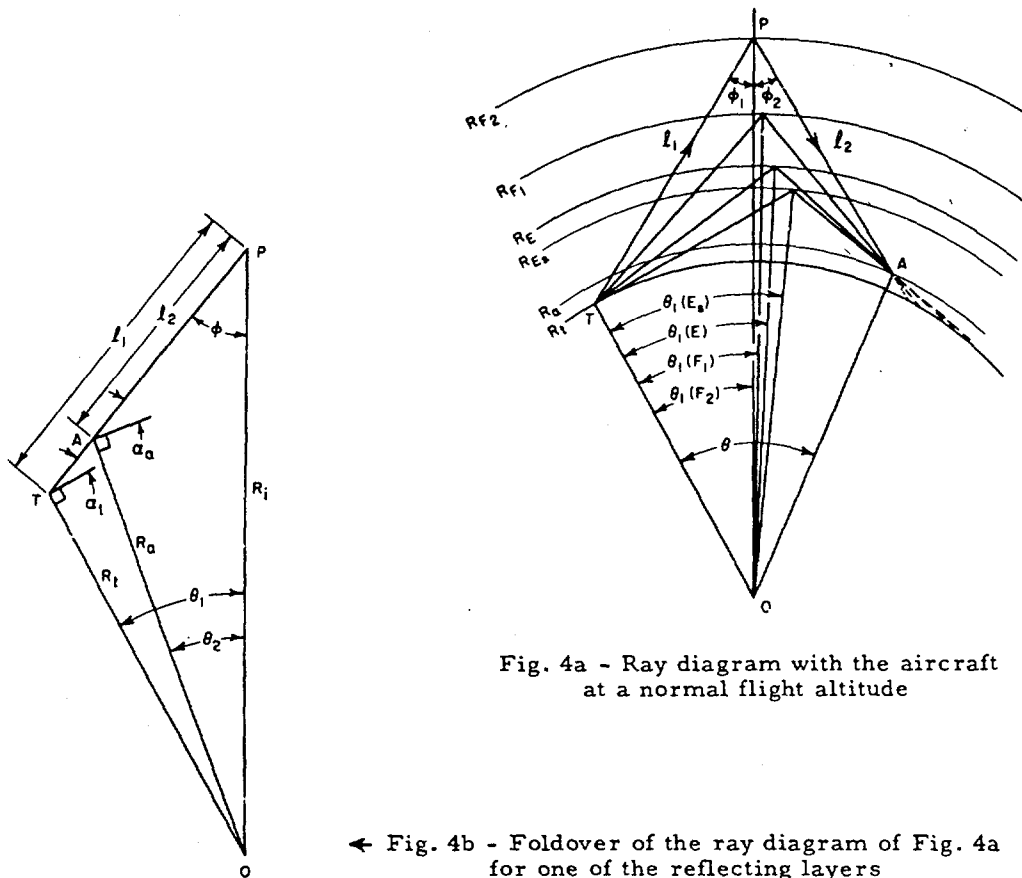
Fig. 4a - Ray diagram with the aircraft
at a normal flight altitude

← Fig. 4b - Foldover of the ray diagram of Fig. 4a
for one of the reflecting layers

In making the calculations and the comparisons it was assumed that the aircraft navigator knew his exact geographical position; it is realized this is subject to an error of at least ±4 miles. Even if the reported position is absolutely correct, time roundoff of a half minute at jet speeds can give a ±4-mile error. Second, a spherical earth was assumed, which can generate an error of several miles. Third, it was assumed that the combined accuracy of the Madre indicator calibration and the operator's interpretation was within 1 mile. Even though the assumptions made are subject to gross errors that can add up to ±15 miles, it was possible to catalog the data into nine out of the ten possible paths. It is realized that an oversimplified picture of the ionosphere has been taken and that some of the paths give ranges within 2 miles of each other. This is particularly true of paths involving E and E_s.

Figure 5 is a time vs range plot showing the range data taken as circles. The dashed line originating at the earliest point is the path predicted for the aircraft from its velocity measured at this time. The solid line is the presumed actual path of the aircraft as calculated from the navigator's record. All points except the two labeled ⊗ are thought to be from the target aircraft; exclusion of these two will be explained later. Figures 6a through 6i are time vs range plots of the observations grouped according to the ionospheric layer(s) rendering the signals, as follows: 6a, E_s; 6b, $E_s + E$; 6c, E; 6d, $E_s + F_1$; 6e, $E + F_1$; 6f, F_1; 6g, $E + F_2$; 6h, $F_1 + F_2$; and 6i, F_2.
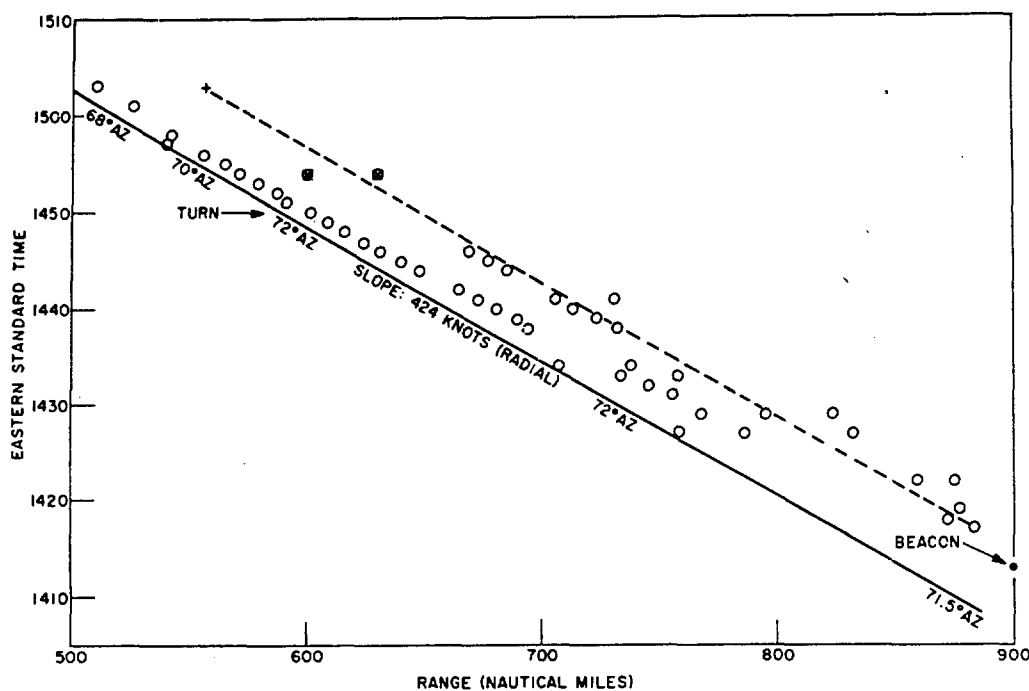
Fig. 5 - Time vs range plot of all data taken on the KC-135
aircraft. The dashed line is predicted from the velocity
measured at the earliest point (slant range); the solid line
is calculated from the navigator's data (ground range). The
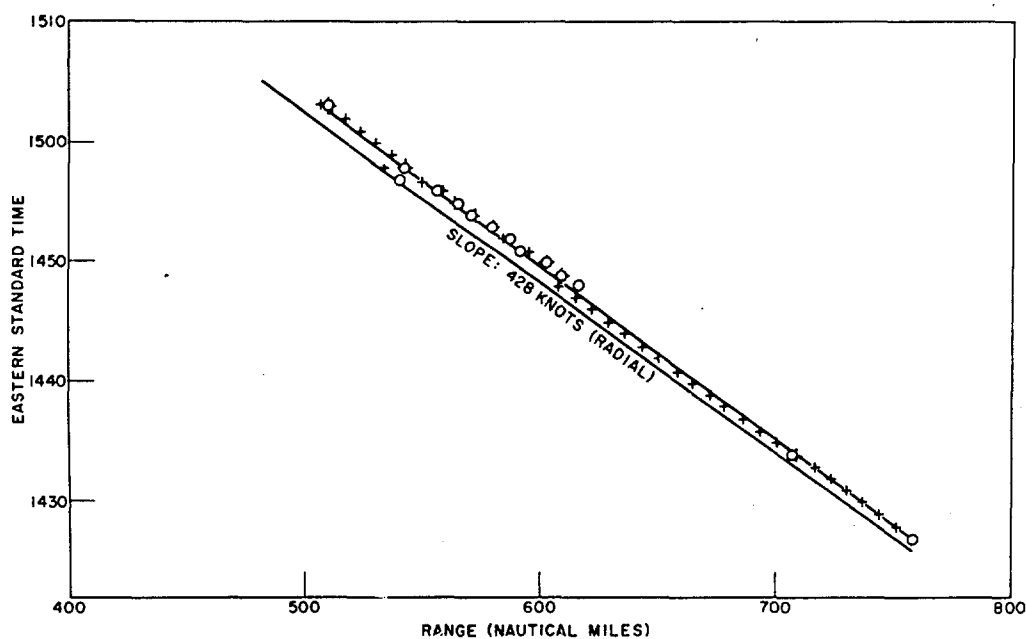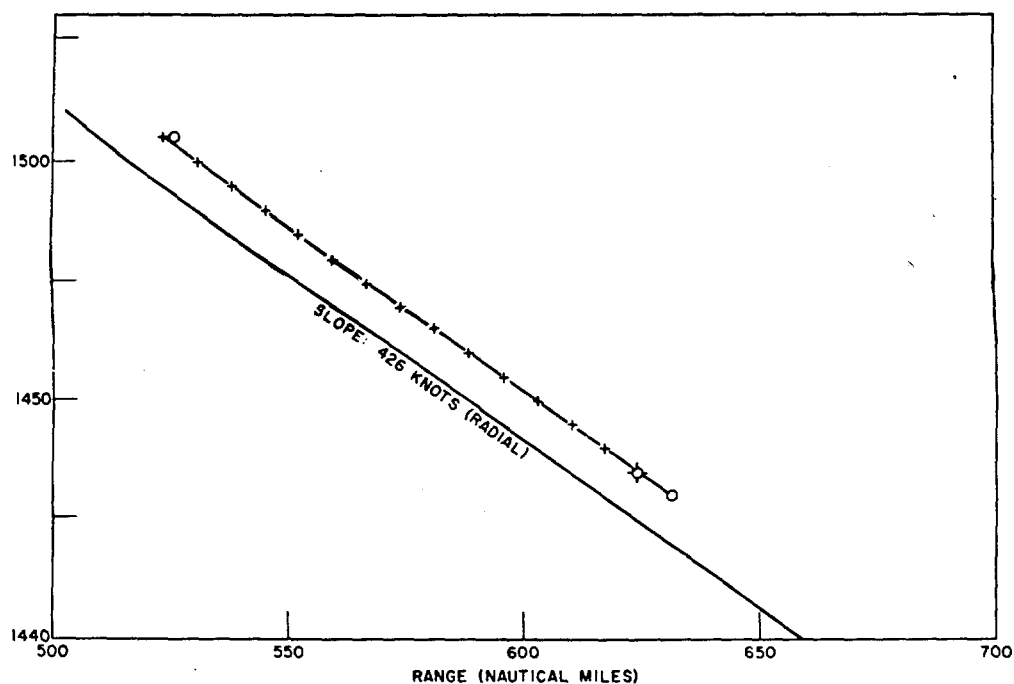calculated radial speeds were 376 to 453 knots.

Fig. 6a - Time vs range plot of points attributed to E_s layer
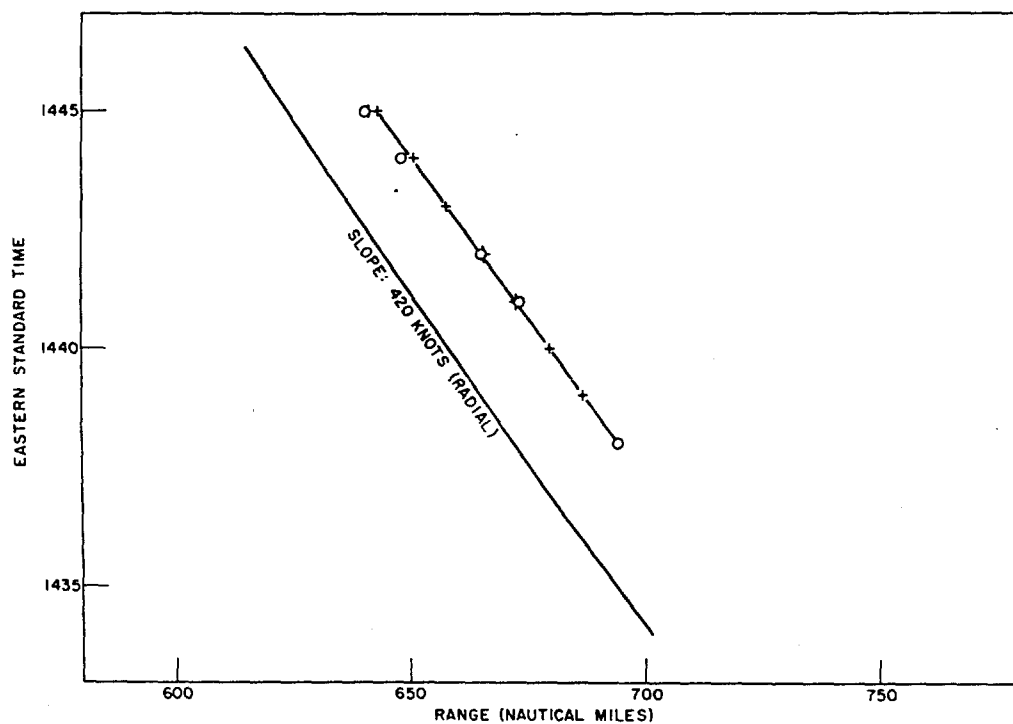reflections. The calculated radial speeds were 376 to 434
knots. The crosses are predicted ranges at 1-minute inter-
vals from the last observation.

Fig. 6b - Time vs range plot of points attributed to E_s + E layer
reflections. The calculated radial speeds were 376 to 430 knots.

Fig. 6c - Time vs range plot of points attributed to.
E layer reflections. The calculated radial speeds
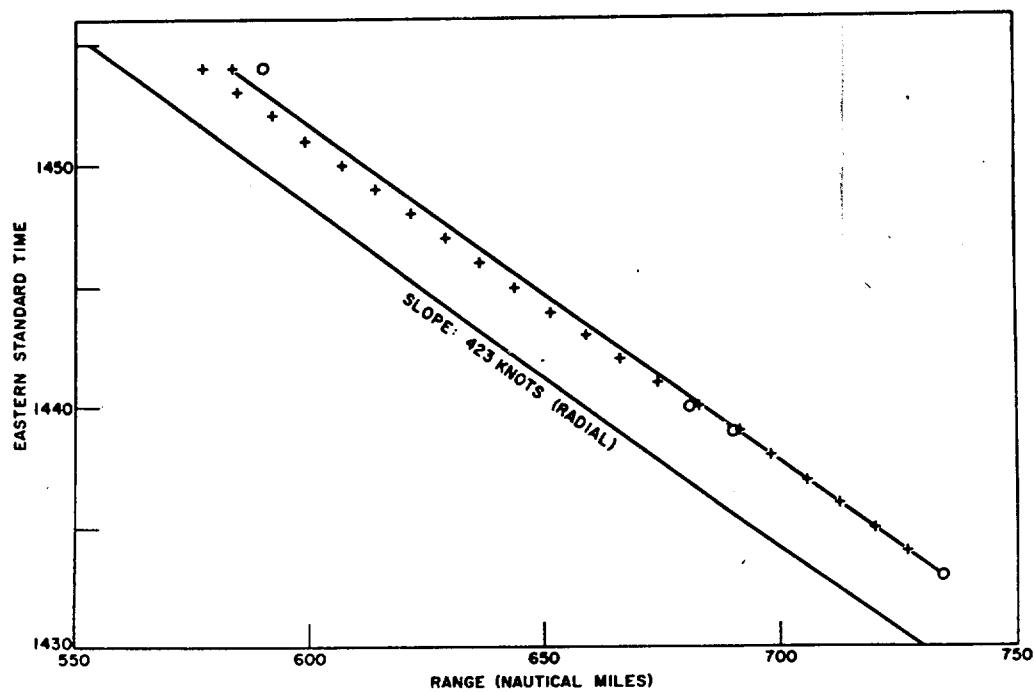were 432 to 441 knots.

Fig. 6d - Time vs range plot of points attributed to $E_s + F_1$ layer reflections. The calculated radial speeds were 413 to 446 knots.
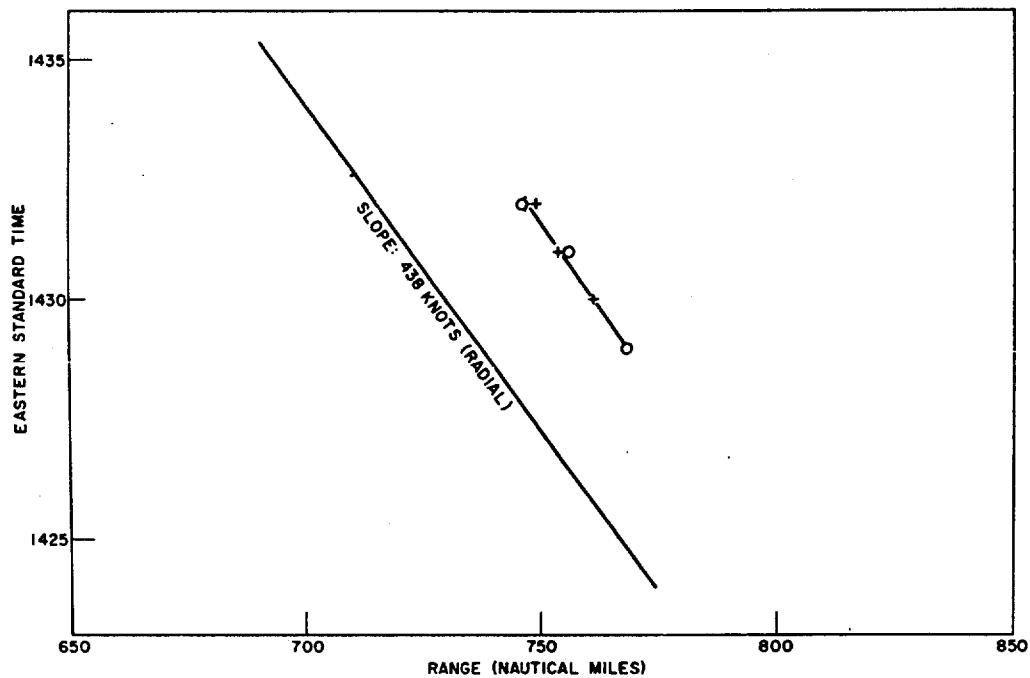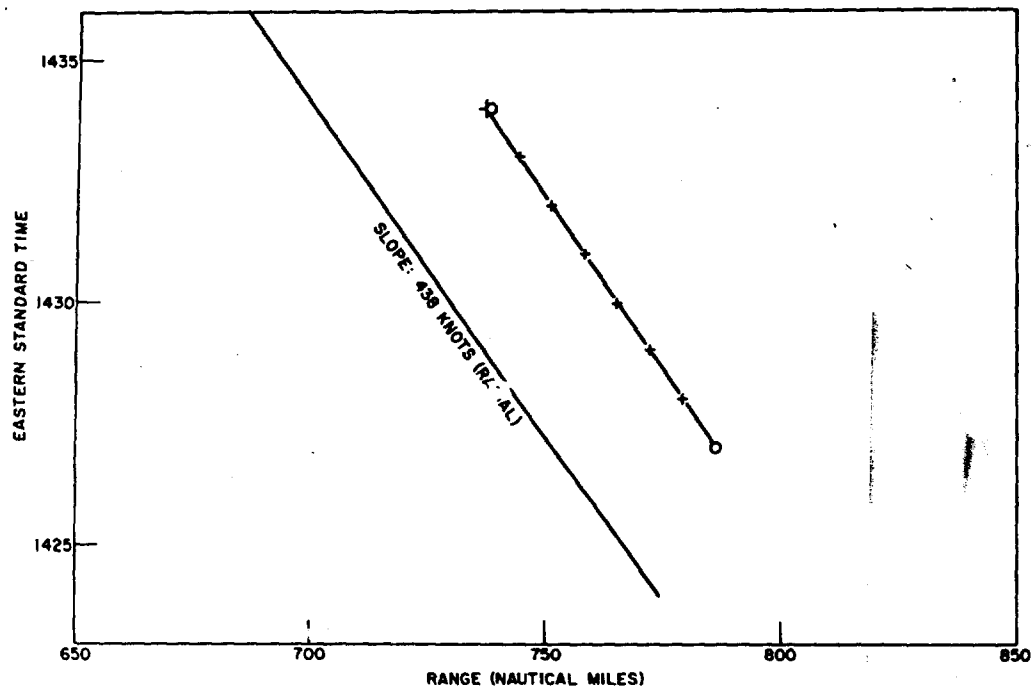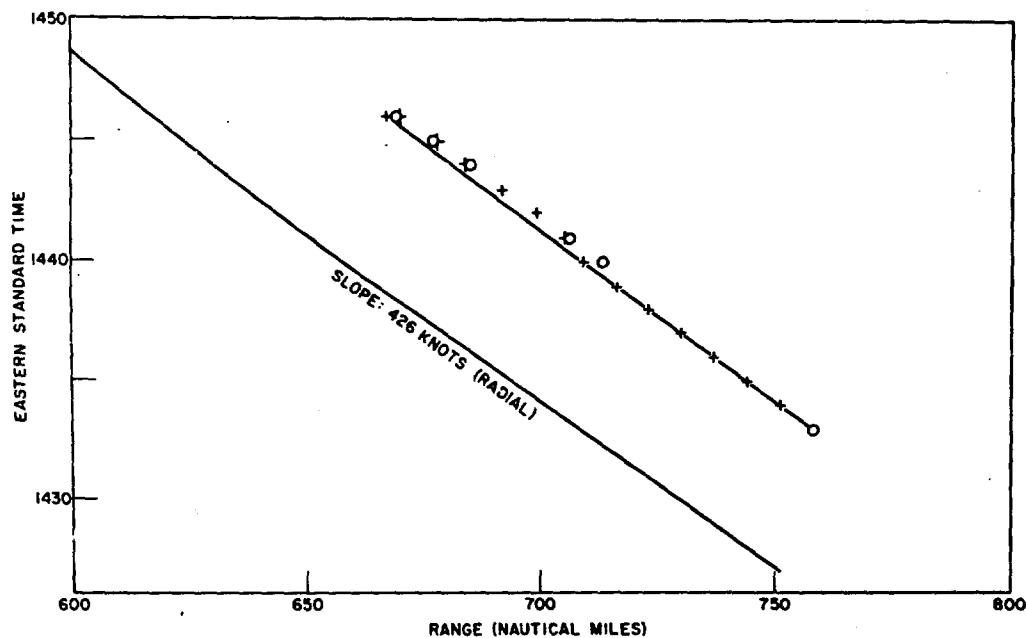

Fig. 6e - Time vs range plot of points attributed to $E + F_1$ layer reflections. The calculated radial speeds were 423 to 426 knots.

NAVAL RESEARCH LABORATORY

Fig. 6f - Time vs range plot of points attributed to
F_1 layer reflections. The calculated radial speeds
were 420 and 426 knots.

Fig. 6g - Time vs range plot of points attributed
to $E + F_2$ layer reflections. The calculated radial
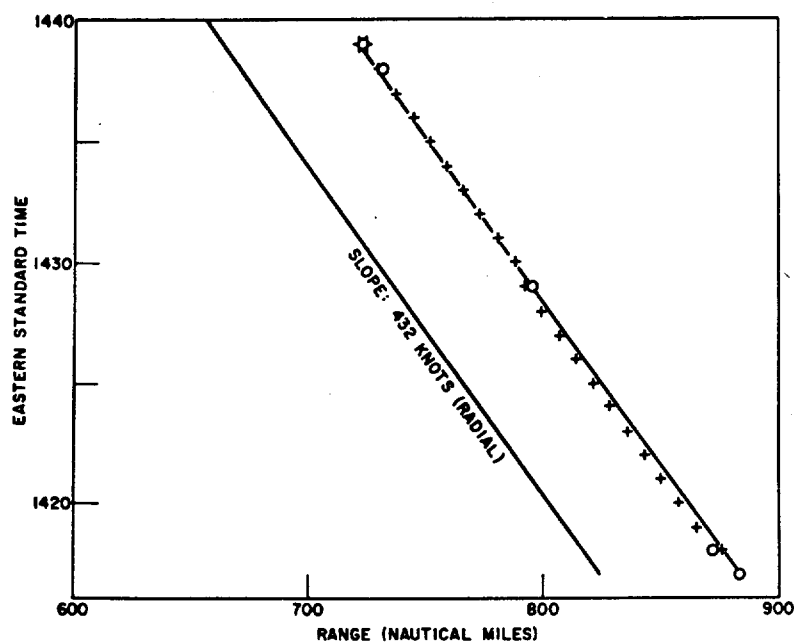speeds were 419 to 445 knots.

Fig. 6h - Time vs range plot of points attributed to $F_1 + F_2$ layer reflections. The calculated radial speeds were 427 to 453 knots.
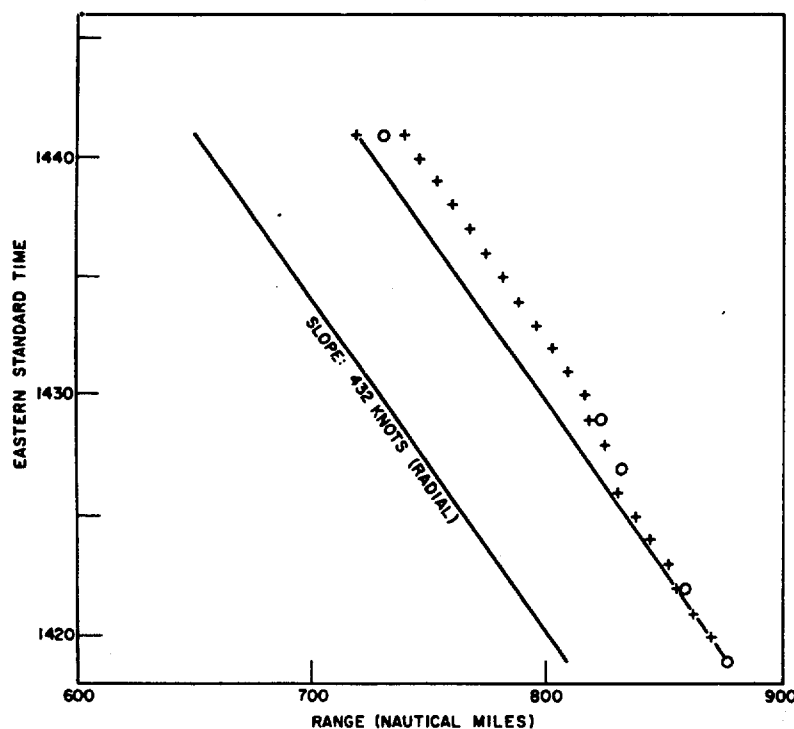

Fig. 6i - Time vs range plot of points attributed to F_2 layer reflections. The calculated radial speeds were 417 to 441 knots.
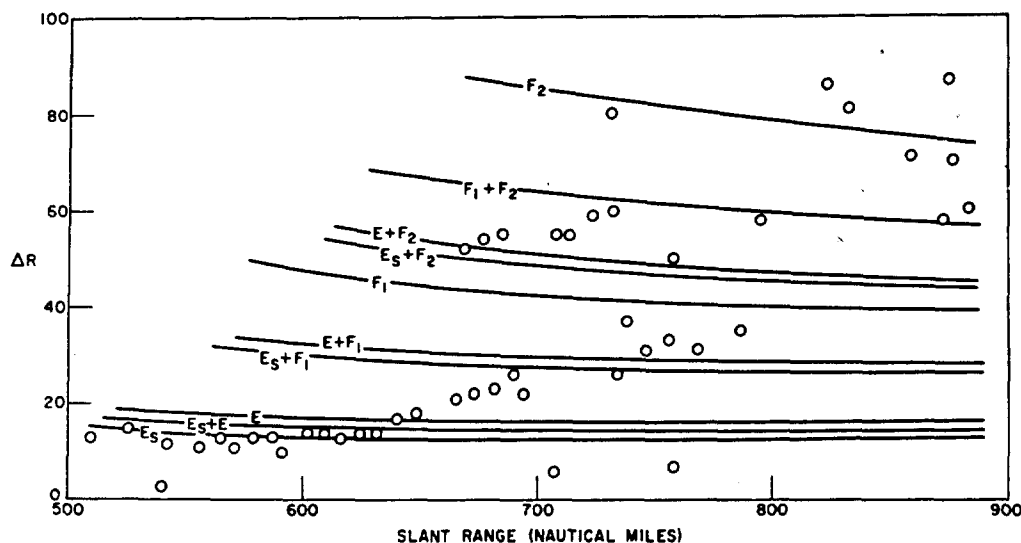
Fig. 7 - Plot of ΔR (slant range minus over-the-ground
range) vs the slant range for the data points in compar-
ison with calculated curves for the various reflection
paths involved

The basis for layer assignment in Figs. 6a through 6i is shown in Fig. 7, a plot of ΔR
vs slant range, where ΔR is slant range minus over-the-ground range. Here the solid lines
represent geometrically determined constant height paths, while the circles represent
signals observed. Layer assignment was made by selecting the path nearest to each obser-
vation. It is apparent that for constant height reflection the range separation ΔR increases
with decreasing slant range. For single-layer propagation conditions one would then expect
a time vs range plot to show the aircraft path and radar track as diverging with decreasing
range.

It is interesting to note that the data plotted in Figs. 5 and 7 clearly show the converse;
the minimum separation is about 58 naut mi for slant ranges greater than 800 naut mi, while
for slant ranges less than 660 naut mi the separation is never greater than 20 naut mi. The
temptation to draw straight lines through the points must be avoided, because it can lead to
erroneous conclusions. For example, from about 600 miles to 690 miles there are eleven
points which lie very nearly along a straight line. Extension of this straight line toward
zero range leads to the conclusion that there is zero range separation at about 550 naut mi
range, and that slant range is less than over-the-ground range between 550 naut mi and
zero range, a condition requiring underground (tunnel) operation of either beam or aircraft.
However, the apparent convergence of slant range and ground range is readily explained on
the basis of path selection if one assumes that lower paths were responsible for reflections
at shorter ranges, or that the returns shifted from F_1 to E_s with all intermediate paths being
represented. This transition is to be expected because of the vertical angle of path. As the
ground distance decreases, the increasing vertical angle approaches the critical angle, at
which the layer stops reflecting. Since the higher layers represent larger vertical angles,
the critical angle should be reached at greater ground ranges for the upper layers than for
the lower layers, and thus the beam would shift successively from higher to lower layers
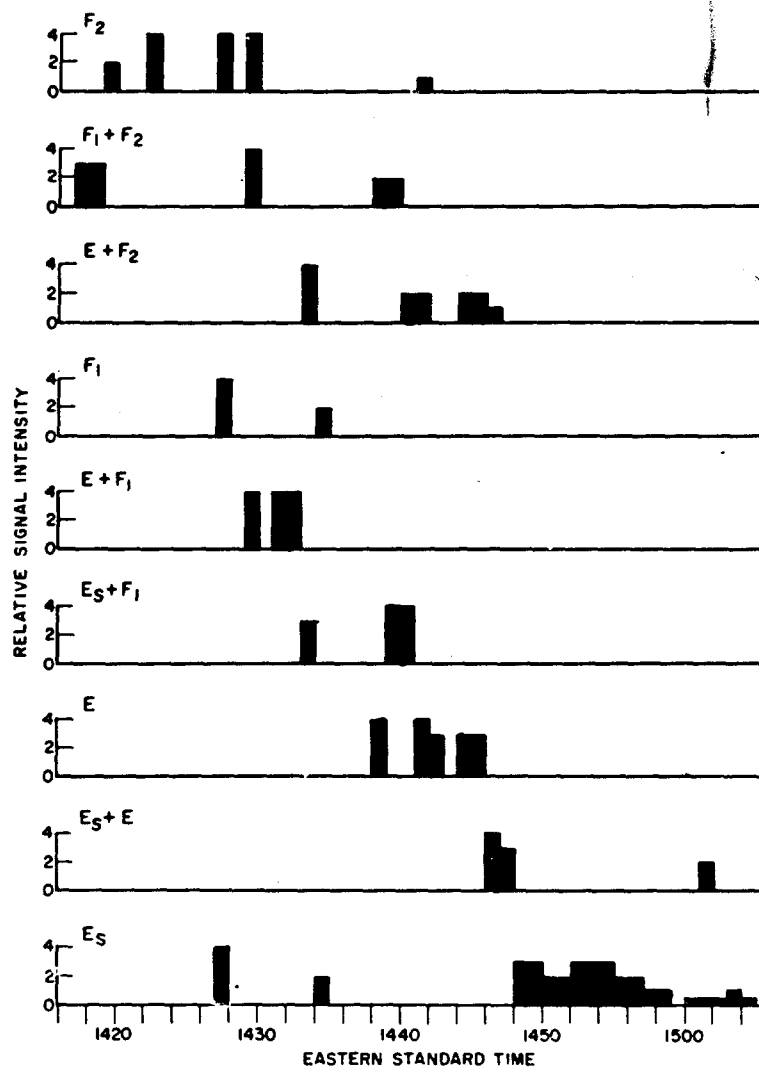as the ground range decreases.

Fig. 8 - Relative signal intensity (nonlinear scale)
during 1-minute intervals

Figure 8 is a plot of the relative signal intensity, on a nonlinear scale of 0 to 4, for the data separated into the various paths. Again the layer succession from higher to lower is apparent.

The all-path relative signal intensity vs time plot (Fig. 9) shows a decreasing intensity starting at about 1447 EST. Although as shown by the azimuths noted in the time vs range plot, Fig. 5, the aircraft started to turn away from beam center rather rapidly at 1450 EST, the signal decline cannot be totally ascribed to the azimuth divergence. Other factors are undoubtedly present, among them the following:

1. The aircraft was departing the illuminated region, since at 1510 EST the start of the backscatter was at 560 naut mi slant range.
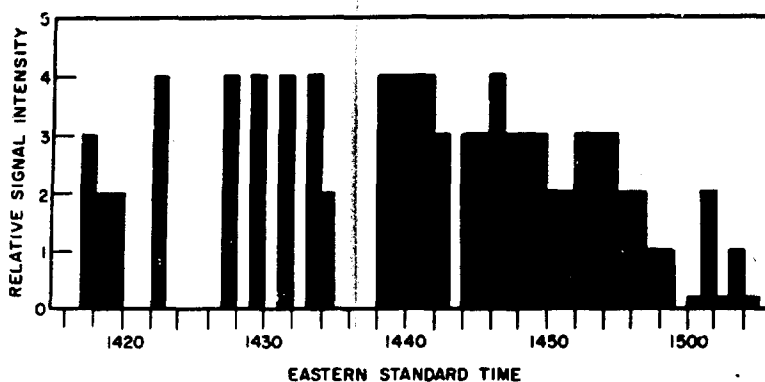
Fig. 9 - Relative signal intensity for all paths

2. Reflection was predominantly from E_s after 1447 EST, from other layers before that time.

A comparison between over-the-ground range as calculated from the navigator's data and as calculated from the radar and ionospheric data is plotted in Fig. 10. The layers thought to reflect each signal are indicated by the symbols as noted on the plot. Here it is seen that the maximum deviation is +13 miles to -11 miles, which is in good agreement with the expected deviation of ±15 miles. The average deviation is 3.28 miles and the arithmetic mean of all deviations is -0.17 mile.
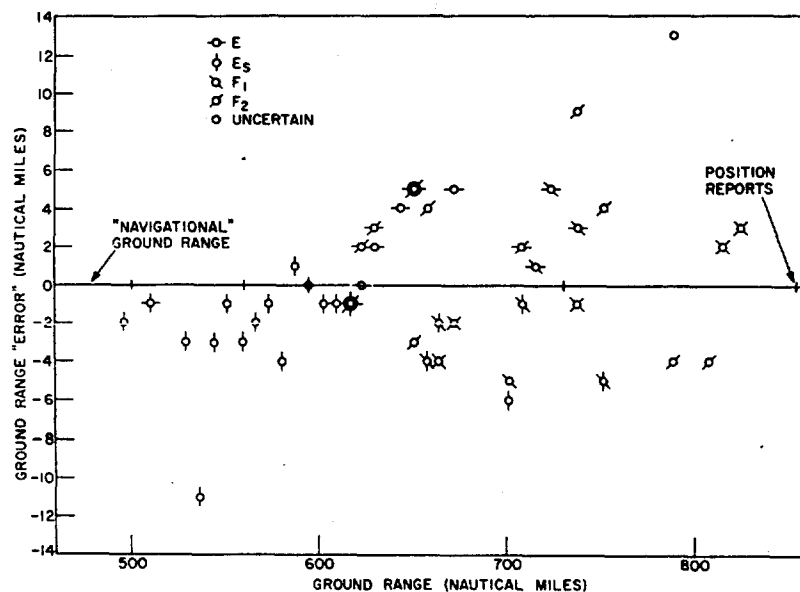

Fig. 10 - "Error" is the ground range derived from the slant range observations (using the assumed layer heights)

The path length necessary for the ray to travel upward to the ionosphere and down again results in indicated ranges which are always slightly greater than the great circle ground distances along the earth's surface to the target.

Likewise, since the speed observed by the radar is the in-line-of-beam component of the aircraft's velocity relative to the antenna, and since all rays except grazing arrive at the aircraft at angles above the horizontal, the indicated speeds should always be less than the radial surface speed. As shown in Fig. 11, the indicated speed is the radial surface velocity times the cosine of the angle of arrival of the ray at the aircraft.

α = ANGLE OF ARRIVAL (ABOVE HORIZON)
OF RAY AT THE AIRCRAFT

V_R = RADIAL COMPONENT OF AIRCRAFT VELOCITY
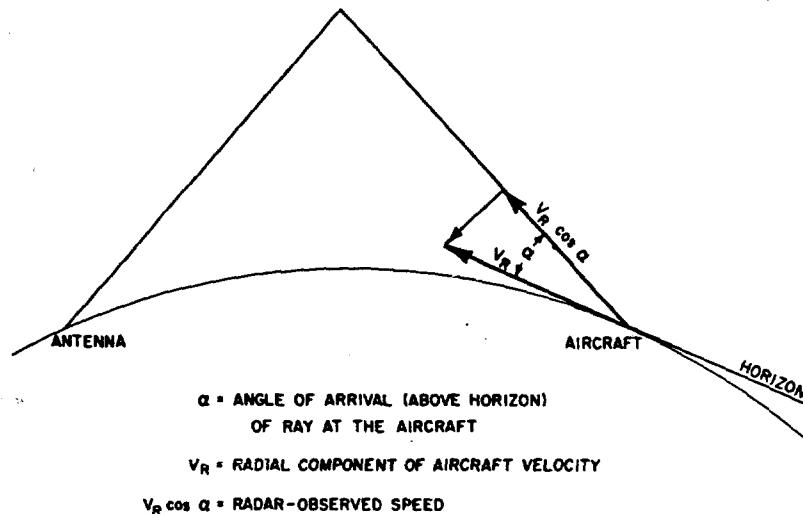
$V_R \cos \alpha$ = RADAR-OBSERVED SPEED

Fig. 11 - Relationship between the measured speed
(range rate) and the ground speed of the aircraft

The radial ground velocity was computed from the measured speeds using the cosine relationship with the angles of arrival obtained from the ionosphere computations. The calculated radial ground speed at 1-minute intervals is plotted in Fig. 12. The solid line connects the average ground speed for every active minute of data. The navigator's data gave an average radial ground speed of 424 miles, the radar data an average ground speed of 423 miles. Since the "sampling" time, at 20 seconds per observation, was only 1/3 of the elapsed time, this agreement is far closer than expected.

At 1454 EST at ranges of 571, 600, and 630 naut mi a target or targets were indicated (Fig. 5). The speeds associated with these ranges were 390, 399, and 397 knots, respectively. The only way one target can have different simultaneous slant ranges is to have reflection from more than one layer, with the longer ranges being from higher layers, and at larger angles of arrival. These higher rays must indicate lower speeds. Although the three readings were taken sequentially within the minute and thus the simultaniety is not exact, a rapid and drastic speed change would have to be postulated to correlate the second and third readings with the first. But since other readings in the immediate vicinity of this triplet showed highly consistent speeds, such a change is improbable. All other multiple signals in the data conform to the inverse range-speed relationship, and indeed the second
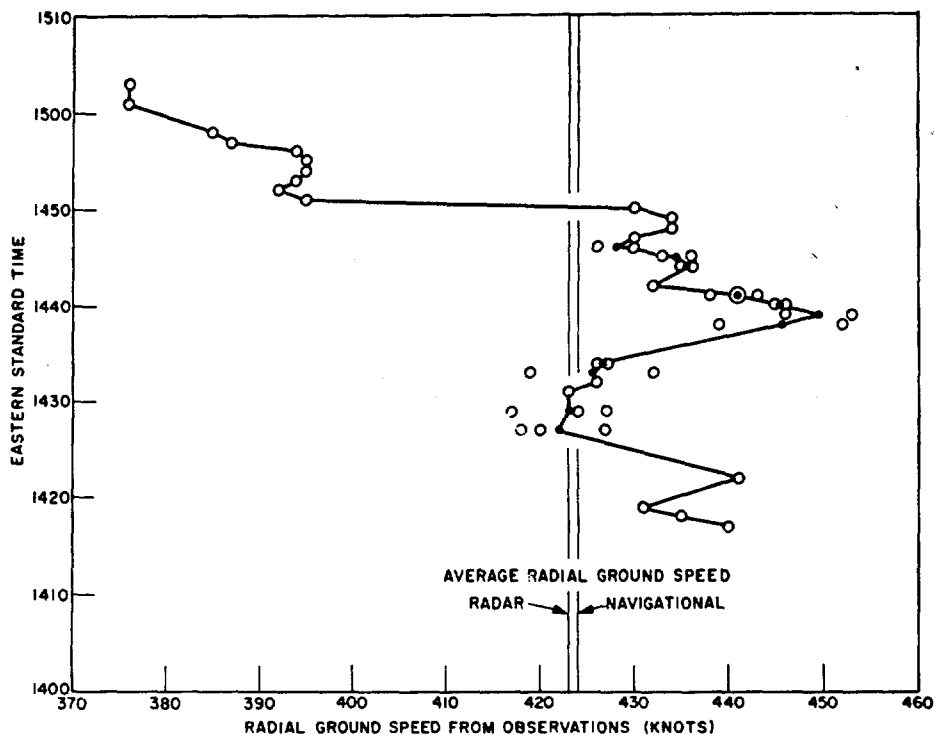
Fig. 12 - Radial ground speeds computed from measured
speeds as shown in Fig. 11

and third points of this triplet conform internally. Therefore, it has been concluded that
these two points cannot be from the target aircraft. Except for these two points, the data
are too consistent to consider that thay are from anything but one target.

Figures 13 and 14 together with Fig. 10 comprise a check on the internal consistency
of the data. Plotted here are the navigation ground range as zero deviation. As described
earlier, Fig. 10 represents the error in ground range vs ground range, as inferred from
indicated (slant) ranges with an idealized four-layer ionosphere. This plot is independent
of speed observations. Figure 13 is the ground range error vs ground range of a hypothet-
ical aircraft which was chosen to be at the target aircraft's position at the time of the first
observation, and whose position was varied each minute consistent with the most recent
speed observation. Since the indicated speeds are slightly lower than true radial surface
speeds, this plot has to show a positive error (ranges greater than "true" ranges) for an
approaching target. This plot is independent of range observations. Figure 14 was con-
structed in like manner, except that instead of using indicated speeds the calculated radial
surface speeds were used to vary the aircraft's position. The calculations to obtain these
speeds were based on both range and speed observations, and this plot is considered a
reasonable composite of the range-derived and speed-derived plots. Ranges at which the
aircraft calculated and reported its positions are indicated by short vertical lines on the
plot, since these may be construed to be the ranges at which the "0" error for navigational
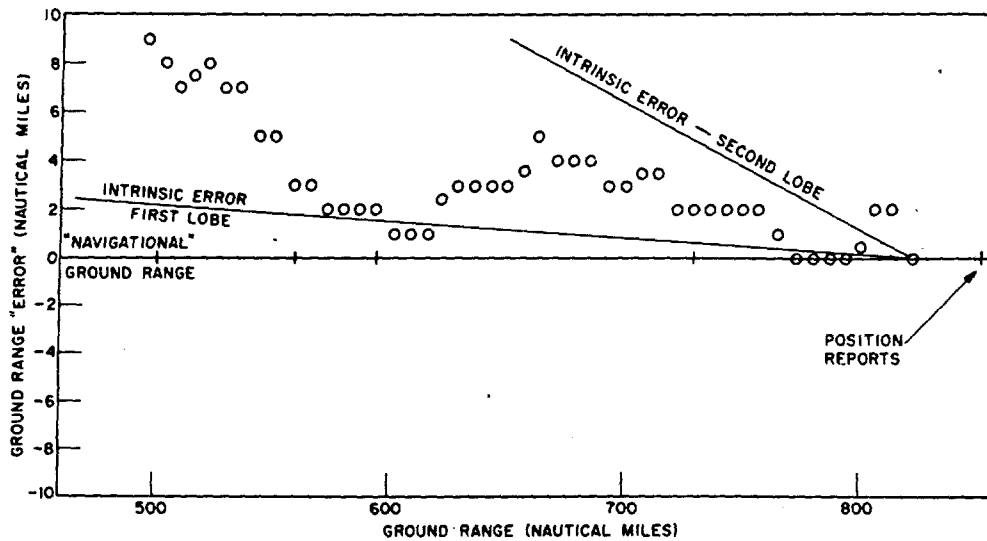ground range is most nearly correct.

Fig. 13 - "Error" in the ground range derived from
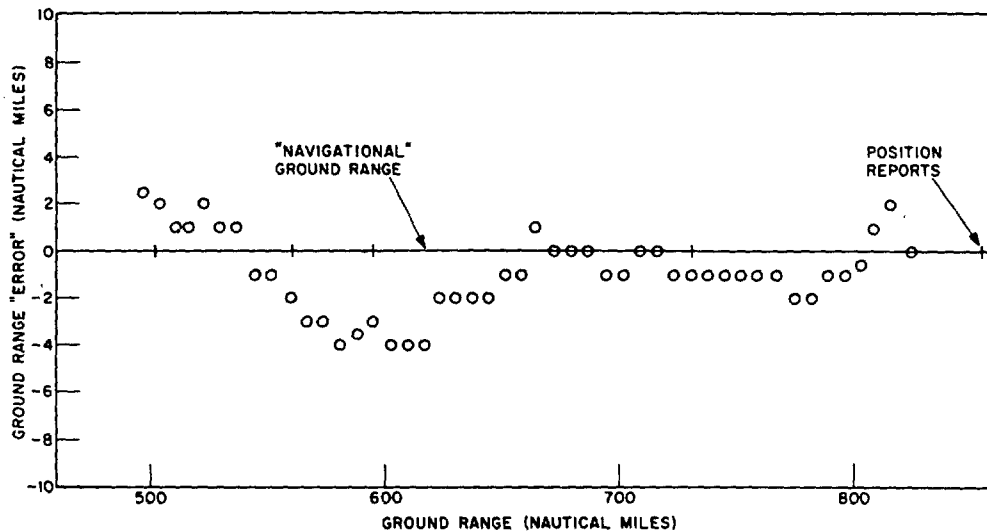range rate observations

Fig. 14 - "Error" in the ground range derived from
calculated radial ground speeds

The arithmetic mean, average deviation, and standard deviation of Figs. 10, 13, and 14 are shown in Table 1. It is seen that range and speed observations, taken separately or together, yield target position information which is well within the ±15-naut-mi "probable error" estimate.

Table 1
The Mean and Deviations of Figs. 10, 13, and 14

Position Information Source	Arithmetic Mean of Errors (naut mi)	Average Deviation (naut mi)	Standard Deviation (naut mi)
Speed Observations (Fig. 13)	+3.11	3.11	3.87
Range Observations (Fig. 10)	-0.17	3.28	4.19
Composite (Fig. 14)	-0.9255	1.54	1.91

Two receiver terminal target signal levels were measured. At 655 naut mi a signal level of 5 μv was recorded. At 602 naut mi a signal level of 10 μv was recorded. Using these measurements one can calculate the target cross section σ by use of

$$\sigma = \frac{P_R}{P_T} \frac{(4\pi)^3 R^4}{G^2 \lambda^2}$$

where P_R is the power received, P_T is the power transmitted, R is the range, G is the antenna gain and λ is the wavelength. The antenna gain was corrected for the calculated angle of arrival, but path loss over free space was not taken into account. The computations gave equivalent target areas of 21 and 56 square meters.

The pattern of the antenna gain is determined by the free space pattern as altered by the ray reflected from the ground and being alternately in phase and out of phase as the vertical angle is increased. The calculated antenna pattern vs over-the-ground range for an aircraft flying at 30,000 feet and the ionospheric height used before is shown in Fig. 15. This pattern has been verified using the moon as a target; the nulls of the antenna occur at the calculated points. This supports the selection of ionospheric heights used before except for five points involving F_1, between 650 and 700 miles ground range. Since a null of the pattern occurs at this position one has to postulate a different ionospheric height or that the ionosphere introduces additional phase shift and/or attenuation in one or both of the rays to smear this pattern. However, the agreement of over-the-ground range and aircraft average velocity leads one to support the smearing of the vertical pattern when the ionosphere is used to obtain over-the-horizon detection. The gains shown are for both of these rays being treated identically in their passage through the ionosphere. An aircraft detected over-the-horizon should have a multilobe structure of its own superimposed on the main lobe structure of the radar antenna. There are four rays that can reach the aircraft, as shown in Fig. 16. These give rise to a multilobe structure as shown in Fig. 17. If this condition were present one would expect a fade on this aircraft at about 1-minute intervals. The envelope of the lobe pattern would be the same shape as in Fig. 15 and this would give an additional 12-db system gain at the maxima of the lobe structure. Since the fast fades were not observed on this target, although they have been observed on some targets, one can support the theory that the ionosphere did smear the vertical antenna pattern and, therefore, that the paths chosen are probably correct.

REMARKS

The data presented have shown that in conditions of multipath propagation to a target it is possible to resolve the paths and to obtain good over-the-ground ranges to targets and good true radial speed from the measured values. Multipath conditions do present secondary problems, but the errors are smaller than the pulse length equivalent in miles.
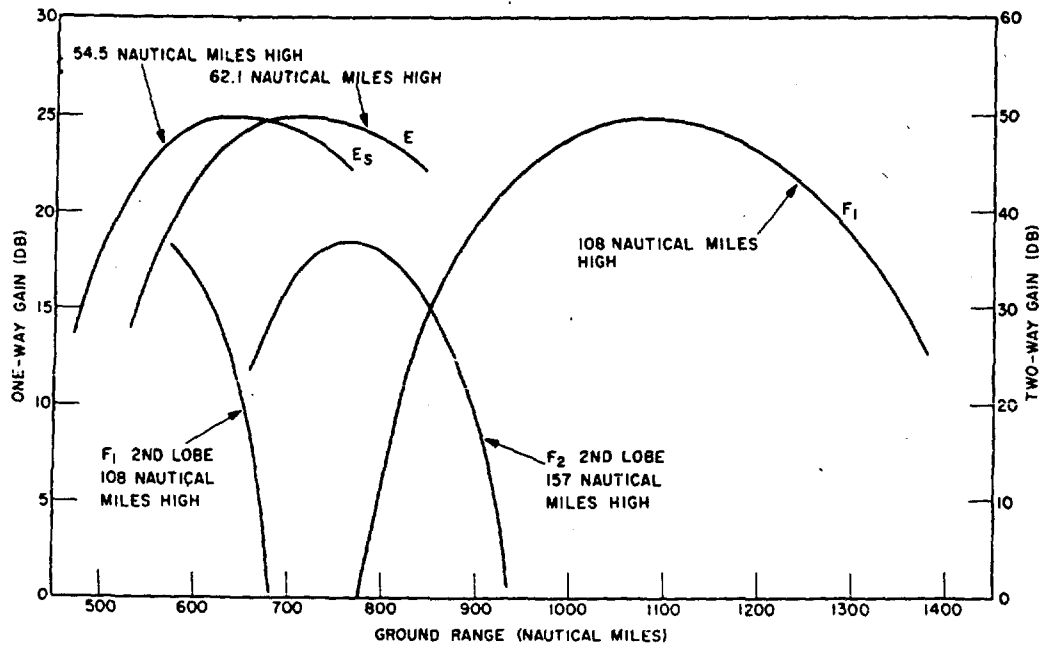
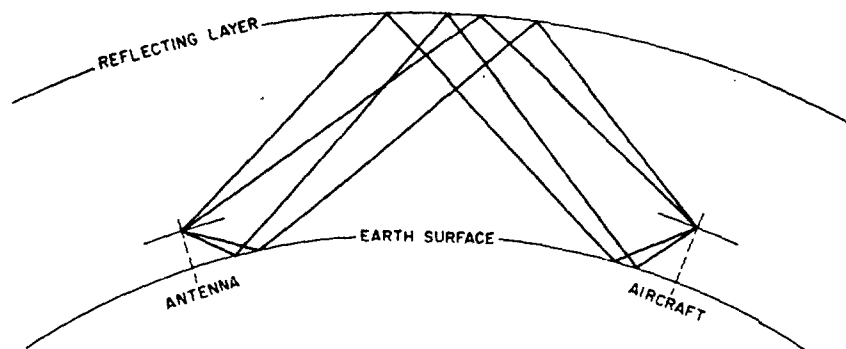Fig. 15 - Antenna gain as referenced to the free space gain

Fig. 16 - Ray diagram of a single-layer reflection
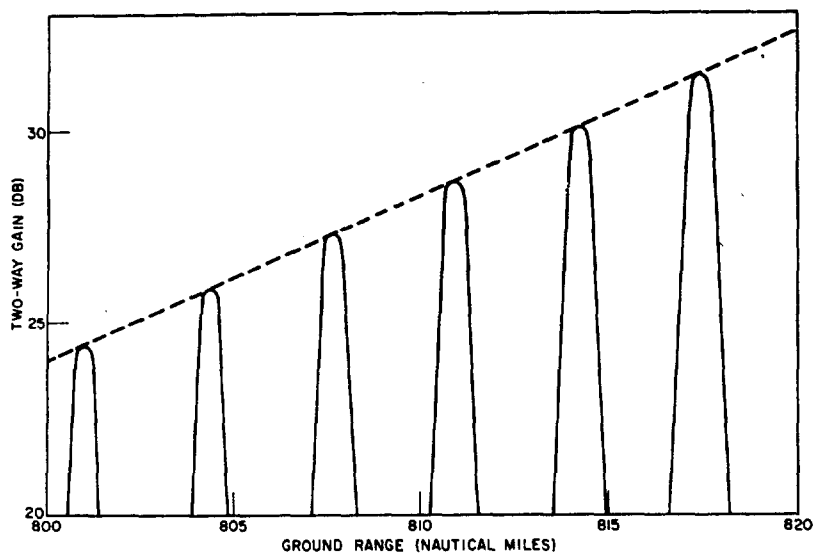showing four paths to the aircraft

Fig. 17 - Fine lobe structure resulting from
the four paths of Fig. 16

ACKNOWLEDGMENT

Operation and maintenance of the Madre equipment requires the skills and services of numerous personnel of the Radar Techniques Branch. The authors acknowledge the expert services and cooperation of F. E. Boyd, J. M. Headrick, and Mrs. Mary E. Thorp. In addition the efforts of the following are commended: Messrs. J. L. Ahearn, E. W. Ward, D. C. Rohlfs, W. B. Patton, G. A. Skaggs, F. E. Wyman, J. P. Wood, C. M. Howe, J. M. Cobble, M. S. Lieberman, and F. H. Utley.

The authors also express appreciation for the cooperation of the USAF's Rome Air Development Center personnel who provided flight assistance.

Naval Research Laboratory. Report 6019 [SECRET] MADRE PERFORMANCE; PART 4 – OBSERVATIONS OF FEBRUARY 15, 1962 [Unclassified Title], by F. M. Gager, G. A. Morgan, W. C. Headrick, C. B. Tesauro, and E. N. Zettle. 22 pp. & figs., January 27, 1964.

The Madre radar was operated on February 15, 1962, to observe a USAF KC-135 aircraft over the North Atlantic Ocean at ranges of 500 to about 900 nautical miles. HF propagation conditions were unusual during the critical portions of the flight, and four ionospheric reflection layers were supported, a situation which provided data for multipath analysis. The analysis shows that in conditions of multipath propagation it is possible to resolve the paths and to obtain good over-the-ground ranges to targets and good true radial speed. Multipath conditions result in recording errors smaller than the range equivalent of the pulse length. [Secret Abstract]

1. Radar systems – Performance
   I. Madre
   II. Gager, F. M.
   III. Morgan, G. A.
   IV. Headrick, W. C.
   V. Tesauro, C. B.
   VI. Zettle, E. N.

Naval Research Laboratory
Technical Library
Research Reports Section

DATE: July 17, 2002

FROM: Mary Templeman, Code 5227

TO: **Code 5300 Paul Hughes**

CC: Tina Smallwood, Code 1221.1 *PH 8/21/02*

SUBJ: Review of NRL Reports

Dear Sir/Madam:

Please review NRL Report 5991 and 6019 for:

☑ Possible Distribution Statement
☑ Possible Change in Classification

Thank you,

Mary Templeman

Mary Templeman
(202)767-3425
maryt@library.nrl.navy.mil

The subject report can be:

☑ Changed to Distribution A (Unlimited)
☑ Changed to Classification *Unclassified*
☐ Other: _____

Paul K. Hughes 4   8/21/200 2
Signature   Date

-- 1 OF 1
-- 1 - AD NUMBER: 344106
-- 2 - FIELDS AND GROUPS: 17/9
-- 3 - ENTRY CLASSIFICATION: UNCLASSIFIED
-- 5 - CORPORATE AUTHOR: NAVAL RESEARCH LAB WASHINGTON D C
-- 6 - UNCLASSIFIED TITLE: MADRE PERFORMANCE. PART 3. OBSERVATIONS
-- OF FEBRUARY 12, 1962. (U)
-- 8 - TITLE CLASSIFICATION: UNCLASSIFIED
-- 9 - DESCRIPTIVE NOTE: INTERIM REPT.,
--10 - PERSONAL AUTHORS: GAGER,F. M. ;MORGAN,G. A. ;TESAURO,CHRISTINE B. ;
-- SKAGGS,G. A. ;ZETTLE,E. N. ;
--11 - REPORT DATE: 30 AUG 1963
--12 - PAGINATION: 16P MEDIA COST: $ 7.00 PRICE CODE: AA
--14 - REPORT NUMBER: NRL-5991
--16 - PROJECT NUMBER: RF001 02 41 4007
--20 - REPORT CLASSIFICATION: CONFIDENTIAL
--22 - LIMITATIONS (ALPHA): NOTICE: ALL RELEASE OF THIS DOCUMENT IS
-- CON-TROLLED. ALL CERTIFIED REQUESTERS SHALL OBTAINRELEASE APPROVAL
-- FROM NAVAL RESEARCH LABORATORY,WASH. 25, D. C.
--23 - DESCRIPTORS: *PERFORMANCE (ENGINEERING)), (*ANTIAIRCRAFT
-- DEFENSE SYSTEMS), (*SEARCH RADAR, PERFORMANCE (ENGINEERING)), RADAR
-- TARGETS, RADAR TRACKING, IDENTIFICATION, TARGET DISCRIMINATION
--24 - DESCRIPTOR CLASSIFICATION: UNCLASSIFIED

--29 - INITIAL INVENTORY: 1
--32 - REGRADE CATEGORY: C
--33 - LIMITATION CODES: 5
--35 - SOURCE CODE: 251950
--36 - ITEM LOCATION: DTIC
--38 - DECLASSIFICATION DATE: OADR
--40 - GEOPOLITICAL CODE: 1100
--41 - TYPE CODE: N
--43 - IAC DOCUMENT TYPE:

UNCLASSIFIED

APPROVED FOR PUBLIC RELEASE - DISTRIBUTION UNLIMITED